

A Model Following Based Real-Time Prediction and Monitoring of TFE-731 Turbofan Engine Compressors

SHIH-HUAI CHEN AND CHAO-CHUNG PENG 

Department of Aeronautics and Astronautics, National Cheng Kung University, Tainan 701, Taiwan

Corresponding author: Chao-Chung Peng (ccpeng@mail.ncku.edu.tw)


This work was supported in part by the Ministry of Science and Technology under Grant MOST 107-2221-E-006-114-MY3 and Grant MOST 108-2923-E-006 -005 -MY3.

ABSTRACT An engine is the heart of an aircraft. It produces thrust, drives the generator, pumps the hydraulic system and provides compressed air for all the systems on the aircraft. Its health plays an essential role in flight safety. In the past, the standard operation procedure to evaluate the health status of engines usually depended on some specific parameters, like inter-stage turbine temperature, low-pressure spool rotating speed or high-pressure spool rotating speed. Once part of the parameters pass over certain safety boundaries that were previously set by the manufacturers or the operators, the engine would be regarded as an unhealthy engine. Nevertheless, in practical applications, such threshold-style mechanism cannot reflect engine fault immediately and therefore could lead to potential flight risk. To solve this issue, a precise forecast model of the engine has to be established. Consequently, this research is dedicated to develop algorithms for engine modeling as well as the identification of optimal parameters. For the TFE-731 engine, there are three section models considered, including low pressure compressor (LPC) model, high pressure compressor (HPC) model and overall turbofan dynamics model. Those models are derived with the consideration of physical isentropic compression equation as well as a data-driven regression technique. Experiments show that a precise modeling fitting can be achieved by using regression analysis and nonlinear optimal parameter estimation. Finally, to compare the prediction stability and accuracy, associated training models using neural network (NN) are also presented. Comparison studies verify that the proposed method is able to achieve stable as well as accurate TFE-731 real-time response prediction and monitoring.

INDEX TERMS Turbofan engine modeling, parameter identification, fault monitoring.

I. INTRODUCTION

The cost of engine maintenance occupies over 30% of the total maintenance cost of an aircraft [1]. If there exists a diagnosis system that is able to monitor the performance, notify where to repair or where to be replaced, or even display the behavior discrepancy in real-time, then the cost of the engine maintenance for both, the military and the airlines can be reduced significantly. In the perspective of engine manufacturers, the current program of engine operation and maintenance budget are performed by a Power by the Hour program. Once the diagnosis system can reduce the time of aircraft on ground, it translates into more profit for the manufactures and the airlines.

The associate editor coordinating the review of this manuscript and approving it for publication was Mark Kok Yew Ng .

Due to lower fuel consumption than turbojet engines, higher and faster flight envelop than turboprop engines, turbofan engines are widely applied to subsonic and supersonic aircrafts [2]. The data used in this research is collected from a TFE-731 test cell. TFE-731 is a two-spool geared turbofan engine consisting of 6 sections. The schematic diagram is illustrated in Figure 1.

TFE-731 comprises the sections of low pressure compressor (LPC), high pressure compressor (HPC), combustion chamber, high pressure turbine (HPT), and low pressure turbine (LPT). Low pressure spool consists of a fan stage, 4-stage axial compressor powered by a 3-stage turbine while a high pressure spool contains a centrifugal compressor powered by the turbine.

The importance of the engine to an aircraft is like that of the heart to a human. In order to increase the flight safety

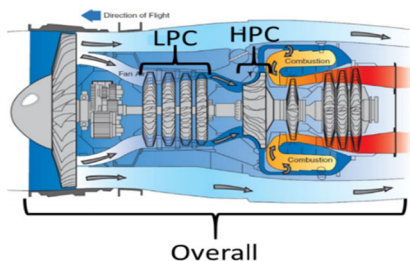


FIGURE 1. The structure of a TFE-731 geared turbofan engine [3].

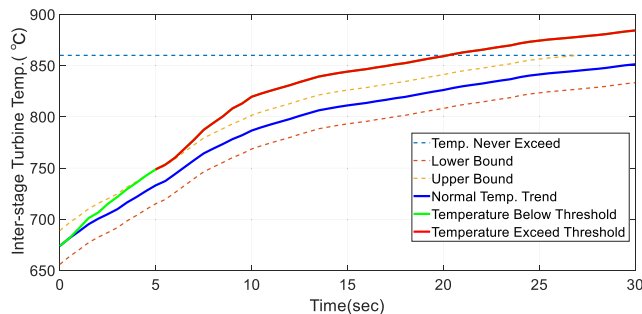


FIGURE 3. Real-time model following based diagnosis method.

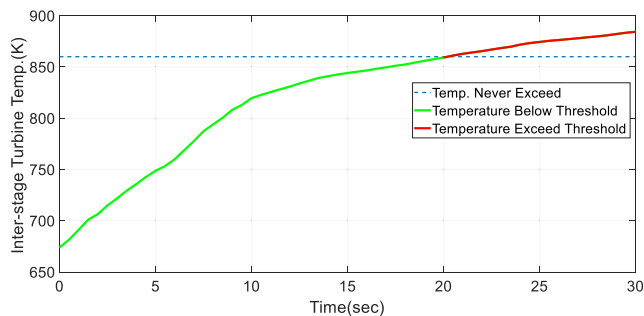


FIGURE 2. Traditional fault diagnosis method.

and to reduce the maintenance cost, there are lots of research focusing on the efficiency, reliability, degradation [4], performance or health monitoring [5], [6], and the life cycle prediction [7], [8]. There is another topic about the sensor fault of aircraft engine presented by Chang [9]. However, due to the demand of real-time system self-awareness and on-line diagnosis increasing, the engine fault message should be triggered and recognized immediately. Recently, a new on-line monitoring strategy has been proposed and verified through wind power systems [10] and multi-axis cutting machines [11], [12]. By using a fraction order chaotic system dynamics feature, the fault condition can be observed easily.

According to the current TFE-731 test cell, a traditional engine fault detection method, as illustrated in Figure 2, is applied. The engine operation terminates only if some specific parameters exceed the prescribed fixed upper or lower limit. Generally, these thresholds are set in advance by designers or field operators. Nevertheless, the engine fault alarm may not be triggered provided the operation testing range is far behind from the threshold. As shown in Figure 3, the traditional method triggers the fault alarm when the engine inter-stage temperature exceeds the presetting upper threshold, color of temperature response changed from green to red. However, the anomaly actually happened for a while. It takes almost 30 seconds delay with respect to the true fault time. Apparently, the traditional method gives rise to potential diagnosis drawback and increases real-time operation risk.

On the contrary, throughout this paper, a model following TFE-731 turbo fan engine real-time diagnosis method is developed. The goals of this work are to notify the field operators immediately to be aware of the engine fault and to point out which section of the engine appears to be failing. As illustrated in Figure 3, once the model following

diagnosis strategy replaces the traditional one, reasonable engine response boundaries are generated accordingly in real-time. Therefore, the algorithm can monitor the anomaly response within a short period of time.

In order to realize this concept, there are three main design steps, including data preprocessing, nonlinear regression model construction and optimal parameter estimation. Data preprocessing makes sure the correctness, usability, correlation and completeness of the data. The procedure of data preprocessing can be divided into parameter arrangement, data usability/completeness check. Next, the nonlinear regression model constructs the physical behavior for different sections of TFE-731 turbofan engine. Finally, optimal parameter estimation is consider to achieve the best fit during the model training.

Regarding the relevant research, it shows that the prerequisite of engine performance monitoring and diagnosis analysis is modeling. Linear parameter varying (LPV) modeling on turbofan engine are presented in [13], [14]. Both Kalman filter [15]–[17] and neural network [18]–[20] are popular methods to recover a complicated physical model. Chang presents a health parameter estimation with second-order sliding mode observer for a turbofan engine [21]. In this work, linear as well as nonlinear engine modeling are considered simultaneously. Regarding the linear modeling, the auto regression and moving average (ARMA) technique is applied. As for the nonlinear system parameter identification, Levenberg-Marquardt (LM) algorithm [22] is designed. The LM algorithm is a popular method to identify the parameters of nonlinear model, which can also been used for modeling the performance of turbofan engine [23], [24].

The predicted models built in this research can be divided into two types: physical based and data-driven model. The physical model is based on the isentropic compression process, fitting the performance of TFE-731 compressors by increasing maneuverability consistence. Data-driven model focuses on the overall engine, in which the fuel flow is taken as the control input signal and the thrust is considered as the output signal. To further increase the accuracy of the prediction model, the concept of Hammerstein system liked method [25], [26] considering the combination of a linear and a nonlinear models are considered. Root mean square error (RMSE), maximum value of error and percent variance

TABLE 1. Key parameters and their logogram.

Logogram	Parameter	Logogram	Parameter
WFA	Fuel flow	FNA	Thrust
TT3	HPC outlet temperature	TT2	Engine inlet temperature
P3	HPC outlet pressure	T235	LPC outlet temperature
N2	High pressure spool rotational speed	P235	LPC outlet temperature
TFANDC	Fan outlet temperature	PT2	Engine inlet pressure
N1	Low pressure spool rotational speed	---	---

accounted for (%VAF) [27], [28] are used to evaluate the performance of the proposed models.

This paper is organized as follows: data preprocessing for parameters arrangement and validation check for modeling are given in Section II. In Section III, methods for the linear and nonlinear equation parameters identifications are introduced. Section IV presents the procedure of TFE-731 modeling, including the sections of the overall engine, LPC and HPC models. Comparison studies between the physical based modeling method and data-drive models by using the popular NN are also considered. In Section V, realization of the real-time TFE-731 condition monitoring is illustrated. In section VI, introduction of the on-line monitoring system application is presented. Finally, Section VII gives a conclusion of the paper.

II. DATA PREPROCESSING

In this research, parameter arrangement and data validation check are considered for data preprocessing. Parameter arrangement focuses on the selection of key engine factors, which is important to the model construction process. Data validation check verifies the correlation between the input signals and the output signals of each section. Only the high correlated data will be selected as the candidate for model training and verification.

A. DATA ARRANGEMENT

Based on the TFE-731 turbofan engine standard operation procedure provides certain important parameters from the core engine, accessory gearbox, and the environment data of the test cell. The key parameters for the sectional engine modeling is shown in TABLE 1.

The main purpose of this research is to predict the operation performance of TFE-731 turbofan engine by using the given data. The sections of the engine modeled in this paper are LPC, HPC, and the performance of the overall engine itself. The input and output parameters used for system modeling and training are defined in TABLE 2.

B. DATA VALIDATION CHECK

Data validation check identifies and isolates the data with abnormal or unreasonable readings in the current database. The abnormal readings might be caused by empty connection of the sensors or the failure of the sensor itself, as illustrated in Figure 4. Figure 4(a) shows the response of power

TABLE 2. The input and output parameters of the models established in this research.

	Inputs	Outputs
LPC	N1, TFANDC, PT2, P235	T235
HPC	N2, TT2, P235, P3	TT3
Overall	WFA	FNA

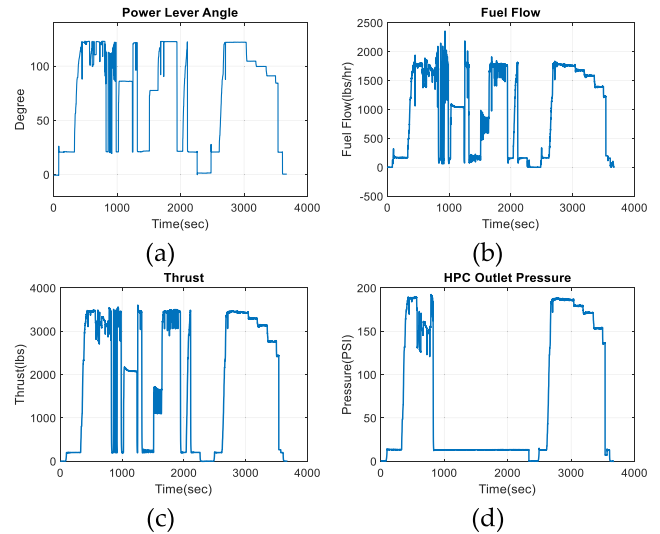


FIGURE 4. Engine testing data with partial unusable P3 (HPC outlet pressure).

lever angle (PLA), which represents the operation input signal manipulated by the local filed operator. The associated fuel flow and engine thrust are given in Figure 4(b) and Figure 4(c), respectively. However, the HPC outlet pressure, as shown in Figure 4(d), shows an extremely low value and it freezes during 800~2300 second. This kind of abnormal responses must be identified and discarded before use.

Since the recorded data might not fit the real outputs closely, then it should be categorized as abnormal data. Subsequently, LPC outlet temperature is considered for the illustration. To recognize the outlier LPC responses, the theoretical outputs of LPC outlet temperature, derived from isentropic compression [2], is considered as following:

$$LPCPR = P_{235}/P_{T2} \tag{1}$$

$$T_{235} = T_{T2} \times LPCPR^{0.3175} \tag{2}$$

where the *LPCPR* denotes low pressure compressor pressure ratio. Generally speaking, the ambient condition for LPC section is outlet temperature and pressure of fan section. However, due to there is no pressure sensor after the fan section in the current TFE-731 test cell, PT2 is considered instead for modeling.

In 2015, Zhao, Dai, and Wang used isentropic compression equation to describe the temperature responses of LPC and HPC section [29].

From the isentropic compression, the outlet temperature of LPC should be strongly related to the low pressure spool rotating speed N1. Therefore, the correlation analysis between T235 and N1 needs to be carried out.

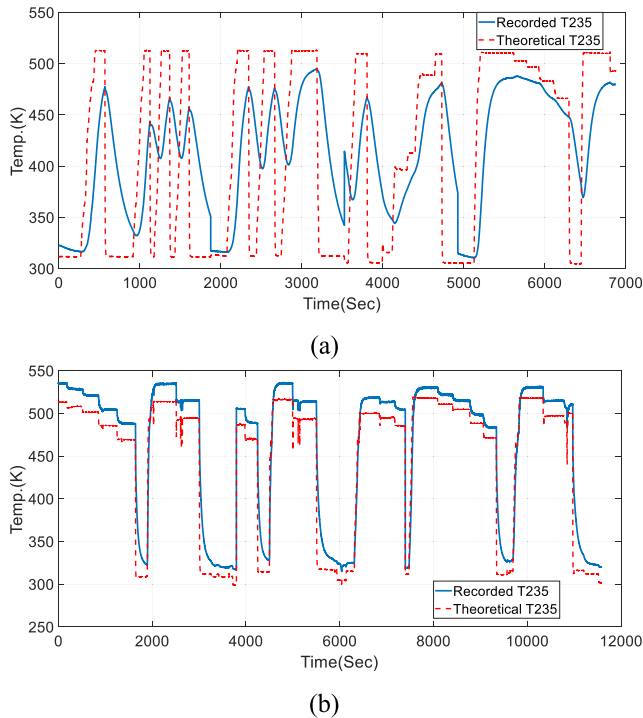


FIGURE 5. The comparison between unusable and usable T235 data and the theoretical outputs: (a) unusable T235 data; (b) usable T235 data.

To achieve this, correlation coefficient, denoted as (3), is applied for the linear relationship evaluations between signals.

$$\eta = \frac{Cov(X, Y)}{\sigma_X \sigma_Y} = \frac{E[(X - \mu_x)(Y - \mu_y)]}{\sqrt{E[(X - \mu_x)^2]} \cdot \sqrt{E[(Y - \mu_y)^2]}} \quad (3)$$

Once the selected signals show a lower correlation than the expected value, they will be considered invalid data, or the outliers.

For example, recorded T235s and TT3 shown in Figure 5(a)/Figure 6(a) and Figure 5(b)/Figure 6(b) are from different dataset. Theoretical output in both figures are calculated by the isentropic compression equation with real engine data. As shown in Figure 5(b), where the solid line represent the recorded T235. The associated correlation coefficient between the theoretical T235 and N1 is 0.9944. But, from another experiment data as shown in Figure 5(a), the correlation coefficient between them is only 0.5011. Therefore, this data is going to be regarded as an abnormal measurement and it will not be included in the training data pool.

On the contrary, a reasonable response is illustrated in Figure 5 (b). It is the comparison between a usable T235 experiment data and the corresponding theoretical value. The correlation coefficient between the real data and the control input is 0.9545; moreover, the correlation coefficient between the theoretical value and the control input is 0.9944. Comparing Figure 5(a)-(b) and Figure 6(a)-(b), it is clear that the T235 and TT3 output displayed in Figure 5(a) and Figure 6(a) has an obvious phase delay and significant

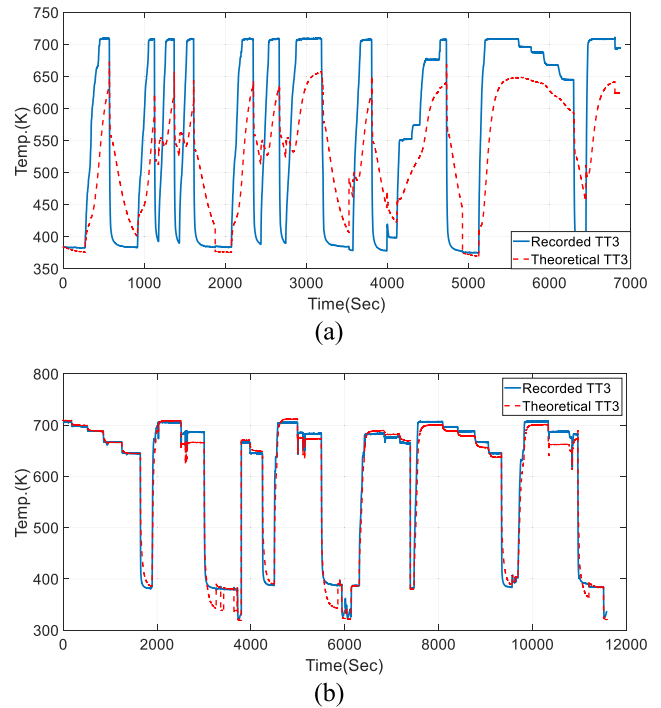


FIGURE 6. The comparison between unusable and usable TT3 data and the theoretical outputs: (a) unusable TT3 data; (b) usable TT3 data.

deviations. Therefore, those data are going to be regarded as invalid data.

Put it simply, for those data, which are quite deviated from the theoretical reference responses, will be identified as outliers and are going to be discarded. The main causes of how those outliers occur include: the degradation of the sensing device, inadequate connection or assembling misalignment of the measurement data acquisition system and so on.

Since the objective of the prediction model establishment is to simulate the reasonable region of a healthy engine in real-time, data usability for the model training has to be verified carefully. This step makes sure the established model can describe the performance of a healthy engine in a proper manner.

III. PARAMETER IDENTIFICATION

After the data effectiveness evaluation, next step is to construct a system model and to identify the associated system parameters. In this section, both the linear and nonlinear parameter identifications are going to be introduced first.

A. LINEAR OPTIMAL PARAMETER IDENTIFICATION

The least square (LS) approach is a popular linear optimal parameter identification method, which could be used to find a set of system parameters. The algorithm minimizes the error between the system output and the reference one. Considering the following linear equation:

$$Y = AX, \quad \begin{cases} Y \in R^{n \times 1} \\ A \in R^{n \times m} \\ X \in R^{m \times 1} \end{cases} \quad n > m \quad (4)$$

Define the estimation error as

$$E = Y - AX \tag{5}$$

The optimal solution is available by applying

$$\min \|E\| = \min \sqrt{E^T E} \Rightarrow \min (E^T E) \tag{6}$$

It is equivalent to finding an optimal solution X_{opt} such that the following quadratic function is minimum

$$\begin{aligned} E^T E |_{X_{opt}} &= (Y - AX_{opt})^T (Y - AX_{opt}) \\ &= Y^T Y - Y^T A X_{opt} - X_{opt}^T A^T Y + X_{opt}^T A^T X_{opt} > 0 \end{aligned} \tag{7}$$

Taking the derivative with respect to X_{opt} gives

$$\frac{\partial E^T E}{\partial X} = -2A^T Y + 2A^T A X_{opt} = 0 \tag{8}$$

It give the well-known LS optimal solution

$$X_{opt} = (A^T A)^{-1} A^T Y \tag{9}$$

B. NONLINEAR OPTIMAL PARAMETER IDENTIFICATION

The LM method [22] is an iterative algorithm for solving nonlinear optimization problems. It could also be used to find a set of local optimal parameters of a nonlinear system to minimize the error between the model and the reference output. LM algorithm is briefly introduced in this section. For the detailed derivation of the LM algorithm, which considers the HPC as an example, please refer to Appendix A.

Regarding the LM algorithm, take $f(\theta)$ as the outputs of the system with a set of unknown parameters θ and let y as the reference performance, the purpose of LM algorithm is to minimize the error between $f(\theta)$ and y . This requirement can be formulated by

$$\begin{aligned} L(\hat{\theta}) &= \arg \min \sum_{n=1}^N (y_n - f_n(\hat{\theta}))^2 \\ &= \arg \min \|y - f_n(\hat{\theta})\|^2 \end{aligned} \tag{10}$$

The optimal solution is expressed by the following iteration process

$$\begin{aligned} f(\hat{\theta}_t) &= f(\hat{\theta}_{t-1} + \delta\hat{\theta}_{t-1}), \\ \delta\hat{\theta} &= \left[(\mathbf{J}^T \mathbf{J} + \lambda \text{diag}(\mathbf{J}^T \mathbf{J})) \right]^{-1} \mathbf{J}^T (y - f) \end{aligned} \tag{11}$$

where \mathbf{J} is the Jacobian matrix of $f(\hat{\theta})$.

IV. TURBOFAN ENGINE MODELING

A. ENGINE OVERALL MODEL

Instead of using the position of PLA as the system input, the fuel flow rate is taken as the input signal of the overall turbo fan dynamic model. For ideal situations, all the important parameters of the engine should be highly correlated with both the PLA and the fuel flow rate. However, if certain defects or uncertainties exist in the test cell, the response of PLA may not be proportional to the generated fuel flow rate. This behavior discrepancy will increase the modeling uncertainties. Due to the reason that the modeling process is based

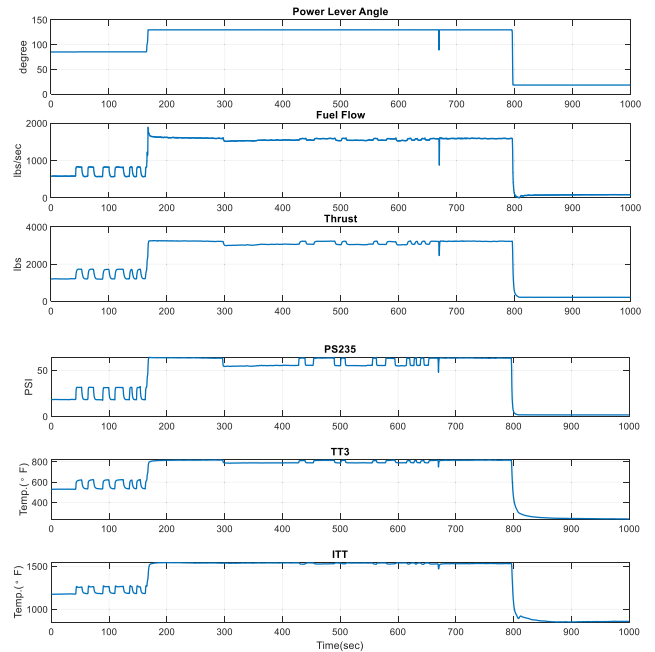


FIGURE 7. The mismatch between power lever angle and other parameters.

on the engines operating on a test cell. The ambient condition is relatively stable than the engines operating on the flying aircrafts. Ambient condition is ignored in the modeling process.

Figure 7 shows a set of recorded data on which the operation of the PLA did not reflect the actual fuel flow rate very well during 180~800 seconds. On the contrary, engine thrust, pressures and temperatures all show high correlations with the fuel flow rate. In other words, there exists no slow frequency vibrations in the PLA signals. In contrast, those vibrations do exist in the fuel flow, thrust, pressures as well as temperatures.

In the following, a regression model that considers the fuel flow rate as the input and the total thrust as the system output is designed. To evaluate fitting performance and to figure out the appropriate order of the regression model, root mean square error (RMSE), maximum error and %VAF [27], [28] are used.

The definition of %VAF is given as follows

$$\%VAF = 100 \times \left[1 - \left(\frac{E \left\{ [(r(t) - \hat{r}(t)) - ((r) - \langle \hat{r} \rangle)]^2 \right\}}{E \{ [r(t) - \langle r \rangle]^2 \}} \right) \right] \tag{12}$$

Based on the ARMA model, Figure 8 shows the identification results. It is shown that the appropriate order of the overall engine regression model is three, which can be expressed in detail as follows

$$\begin{aligned} TR(k) &= X_{opt1}^{overall} \cdot TR(k-1) + X_{opt2}^{overall} \cdot TR(k-2) \\ &\quad + X_{opt3}^{overall} \cdot TR(k-3) + X_{opt4}^{overall} \cdot WFA(k) \\ &\quad + X_{opt5}^{overall} \cdot WFA(k-1) + X_{opt6}^{overall} \cdot WFA(k-2) \\ &\quad + X_{opt7}^{overall} \cdot WFA(k-3) \end{aligned} \tag{13}$$

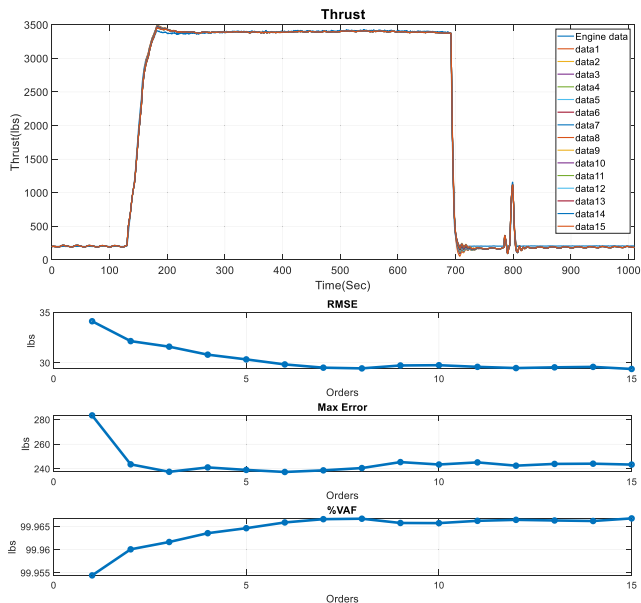


FIGURE 8. The comparison of the overall regression models with different orders and the result of root mean square error, maximum error value and %VAF.

TABLE 3. Parameter identification of different engines.

Engine ID	$X_{opt1}^{overall}$	$X_{opt2}^{overall}$	$X_{opt3}^{overall}$	$X_{opt4}^{overall}$
86124	1.2428	-0.3069	-0.0040	0.9865
53130	1.3503	-0.3910	0.0189	0.8256
54111	1.2825	-0.1830	-0.347	0.3535
Engine ID	$X_{opt5}^{overall}$	$X_{opt6}^{overall}$	$X_{opt7}^{overall}$	---
86124	-0.7087	-0.1964	0.0521	---
53130	-0.6727	-0.0746	-0.0345	---
54111	-0.1873	-0.1054	0.0106	---

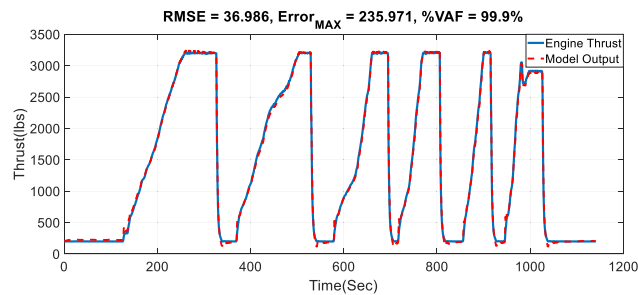
To verify the correctness of the regression model (13), a couple of engines are considered. The associated identified parameters for each engine are listed in TABLE 3.

Figure 9 illustrates the responses and the corresponding fitting results for different TFE-731 turbofan engines under a wide variety of fuel flow rate operations. Those engine operations are based on the test standard procedures, which tend to include all the flight conditions, the maximum thrust and cruising thrust evaluations.

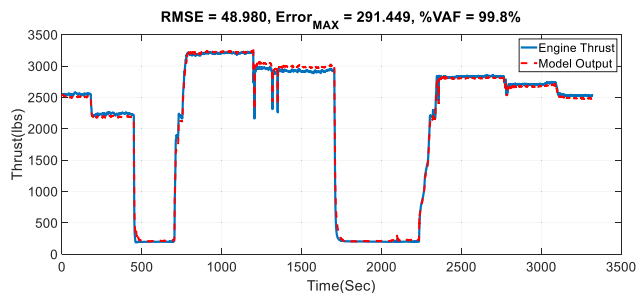
Experiments evidently demonstrate that the third order regression model (13) is able to fulfill engine thrust predictions for TFE-731 turbofan engines, no matter what the serial number or operation procedure is.

B. LPC MODELING

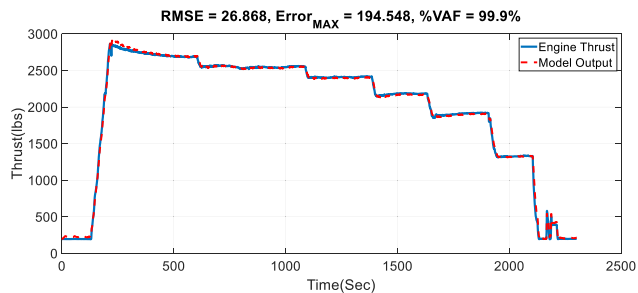
From the theoretical point of view, the outlet temperature of LPC can be calculated by using the isentropic compression equation (1) and (2). Unfortunately, the test cell can never create an ideal test condition. Therefore, in order to get a precise prediction model, the isentropic compression equation has to be further revised. The revised LPC model is proposed



(a)



(b)



(c)

FIGURE 9. Overall model performance between different engines: (a) ID: 86124; (b) ID: 53130; (c) ID: 54111.

TABLE 4. The initial value and the result after the nonlinear optimize iteration for LPC model.

	k_1	k_2	k_3	k_4	k_5	k_6
Initial value	1	0.3175	0	0	0	0
Optimize parameter	1.33	0.29	-0.081	-13.7	1.276	-407

as follows

$$t_{235} = k_1 \times T_{FANDC} \times LPCPR^{k_2} + k_3 \times N_1 + k_4 \times LPCPR + k_5 \times T_{FANDC} + k_6 \quad (14)$$

Eq. (14) shows that the LPC model increases the degree of freedom by considering N_1 , separated LPCPR and TFANDC, and a constant term. It can be taken as an extension version of the theoretical model (1) and (2). However, since (14) is a nonlinear algebra equation, the LS can not be applied. Therefore, the LM algorithm is used for figuring out an optimal set of parameters. The initial values and the corresponding estimates are shown in TABLE 4. The fitting performance is illustrated in Figure 10.

Figure 10 shows that the preliminary LPC model (14) is able to achieve more than 95% VAF of the system response.

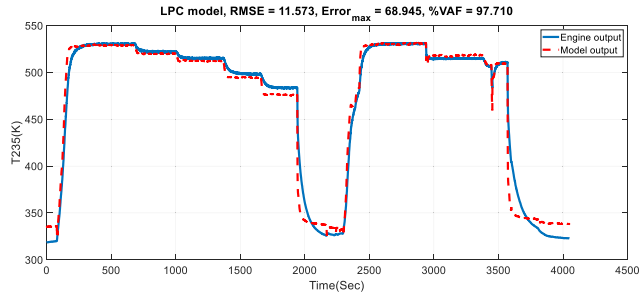


FIGURE 10. LPC model fitting performance by (14).

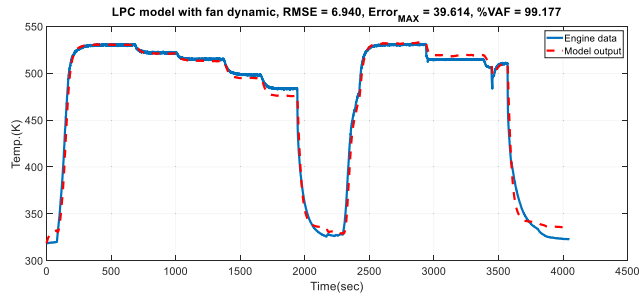


FIGURE 11. LPC model with fan dynamic fitting performance, where $k_1 = 0.9775$, $k_2 = 1.256 \times 10^{-6}$ and $k_3 = 0.0219$.

Owing to the series connection of the fan and the LPC section, a fan dynamic like regression model [30] is considered for the transient response modeling of t_{235}

$$\hat{T}_{235}(k) = x_1 \times \hat{T}_{235}(k-1) + x_2 \times \hat{T}_{235}(k-1)^2 + x_3 \times t_{235}(k) \quad (15)$$

where $\hat{T}_{235}(k)$ represents a new predicted LPC outlet temperature and $t_{235}(k)$ in (14) is taken as the associated driving input.

Based on the concept of Hammerstein cascade system, the performance of the revised LCP model is shown in Figure 11. After combining with the fan regression model, the revised LPC model attenuates both the RMSE and the maximum error while also increasing the %VAF. It evidently verifies that the revised LPC model has a better fitting performance than the former one.

In order to enhance the fitting precision, we further refine the temperature nonlinear regression model (15) by

$$\hat{T}_{235}(k) = x_1 \times \hat{T}_{235}(k-1) + x_2 \times \hat{T}_{235}(k-1)^2 + x_3 \times \hat{T}_{235}(k-1)^3 + x_4 \times t_{235}(k) \quad (16)$$

The associated fitting result is illustrated in Figure 12. Obviously, with the combination of a non-linear isentropic compression equation and a nonlinear regression model, the accuracy of the LPC model is enhanced successfully.

C. HPC MODELING

The main procedures for the modeling of the HPC section are similar to those applied for the LPC model derivation. For the HPC section, the following isentropic equations are first

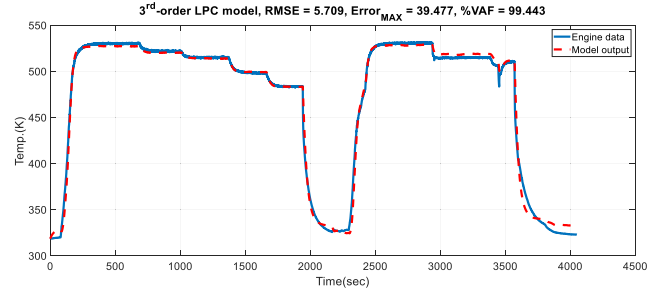


FIGURE 12. The performance of LPC model with a 3rd-order regression model, where $x_1 = 0.9600$, $x_2 = 7.096 \times 10^{-5}$ and $x_4 = 0.0249$.

TABLE 5. The initial value of LM algorithm for HPC model (19) and (20).

	k_1	k_2	k_3	k_4	k_5
DoF _{low}	1	0.3175	0	0	0
DoF _{high}	1	0.3175	0	0	0
	k_6	k_7	k_8	k_9	
DoF _{low}	0	---	---	---	
DoF _{high}	0	0	0	0	

considered as follows

$$HPCPR = P_3/P_{235} \quad (17)$$

$$H_{est} = T_{235} \cdot HPCPR^{0.3175} \quad (18)$$

From (16) and (18), it shows that T_{235} not only represents the outlet temperature of LPC model, but also acts as the inlet temperature of the HPC model.

Similarly, in order to increase the degree of freedom of the isentropic equation (18), the model is extended by two ways as shown in (19) and (20), respectively.

$$H_{est}^{low} = k_1 \times HPCPR^{k_2} + k_3 \times N_2 + k_4 \times T_{235} + k_5 \times HPCPR + k_6 \quad (19)$$

$$H_{est}^{high} = k_1 \times HPCPR^{k_2} \times HPCPR^{k_3} + k_4 \times N_2 + k_5 \times LPCPR + k_6 \times T_{T2} + k_7 \times HPCPR + k_8 \times T_{235} + k_9 \quad (20)$$

Model (20) is the resultant combination of the LPC isentropic compression together with (19) in order to enhance the degree of freedom for dynamics description. The initial value of LM algorithm for model (19) and (20) are given in TABLE 5. The fitting performance comparisons by using different models are illustrated and summarized in Figure 13 and TABLE 6, respectively.

Figure 13(a) shows that the response of the theoretical model can only roughly fit the engine performance, but could not forecast the behavior precisely for the high and low temperature parts. Comparing between the theoretical model and the low degree of freedom model shown in Figure 13(b), model (20) demonstrates a superior predictive performance. Although (20) is able to achieve satisfactory results, the transient behavior can never be properly described. To solve this problem, the following linear regression model is introduced

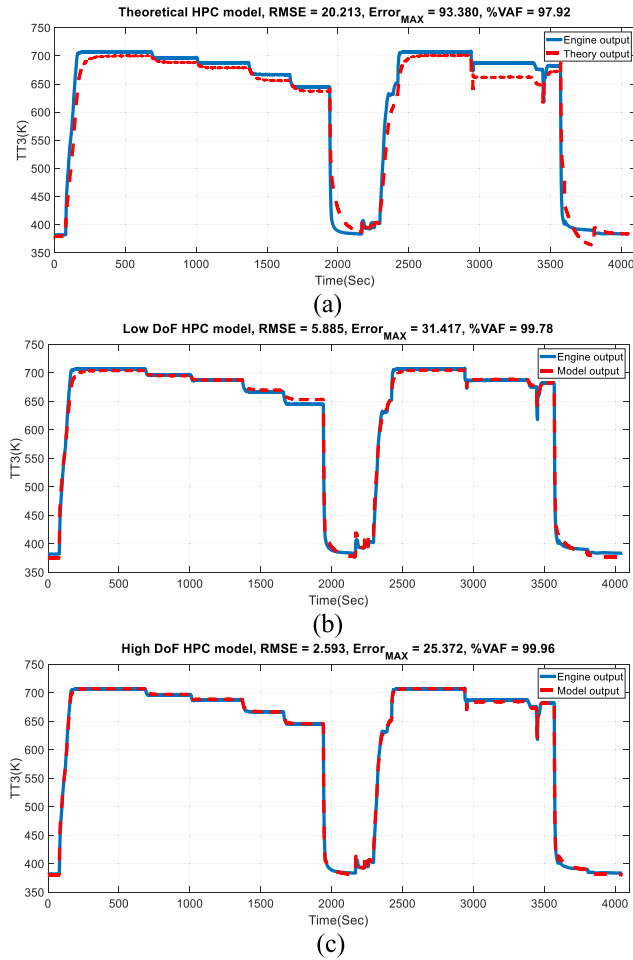


FIGURE 13. Model performance comparison, the models are as: (a) Theoretical model; (b) Low degree of freedom model; (c) High degree of freedom model.

TABLE 6. Model performance comparison.

	RMSE	Max error	%VAF
Theoretical model (H_{est})	20.21	93.38	97.92%
Low DoF model (H_{est}^{low})	5.89	31.42	99.78%
High DoF model (H_{est}^{high})	2.59	25.37	99.96%

in a cascade after (20).

$$\begin{aligned} \hat{T}_{T3}(k) = & X_{opt1}^{HPC} \cdot \hat{T}_{T3}(k-1) + X_{opt2}^{HPC} \cdot \hat{T}_{T3}(k-2) \\ & + X_{opt3}^{HPC} \cdot \hat{T}_{T3}(k-3) + X_{opt4}^{HPC} \cdot H_{est}^{high}(k) \\ & + X_{opt5}^{HPC} \cdot H_{est}^{high}(k-1) + X_{opt6}^{HPC} \cdot H_{est}^{high}(k-2) \\ & + X_{opt7}^{HPC} \cdot H_{est}^{high}(k-3) \end{aligned} \quad (21)$$

where the regression system order is defined automatically by using a similar way to the one presented in Figure 8. The performance of the combined model is shown in Figure 14.

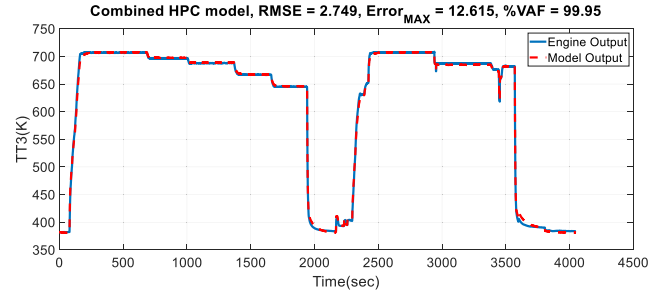


FIGURE 14. The fitting response of the combined HPC model, where $X_{opt1}^{HPC} = 1.2710$, $X_{opt2}^{HPC} = -0.1204$, $X_{opt3}^{HPC} = -0.1586$, $X_{opt4}^{HPC} = 0.5361$, $X_{opt5}^{HPC} = -0.4146$, $X_{opt6}^{HPC} = -0.2286$ and $X_{opt7}^{HPC} = 0.1152$.

TABLE 7. Input and output signal of LPC NARX model.

Input signal	Output signal
TFANDC, LPCPR, N1	T235

Although the RMSE slightly increased and the %VAF slightly degraded, the maximum error value decreased dramatically.

D. NEURAL NETWORK MODEL COMPARISON

In recent years, data driven based NN has become one of the most popular algorithms for system modeling. However, without the aid of physical model behavior, applying the data-driven based NN could not only lead to system parameter burden, but could sometimes give rise to reliable or unstable prediction. Those scenarios are obvious when training samples are not sufficient. Moreover, data generation from real engine test cell are costly and time consuming. It is worth it to pursue and propose a reliable TFE-731 model in the presence of training data insufficiency.

Therefore, in this paper, the TFE-731 models that combine physical compression equations as well as nonlinear regression equations are presented. In the following, the pure data-driven based NN and the proposed method are considered for the comparison study. The LPC model will be taken as the candidate for comparison. It will be demonstrated that the proposed method is able to provide stable and accurate response predictions.

To compare the methods fairly, input signals of NARXs are the same as the presented LPC model. The input and output signal of the LPC NARX model are listed in Table 7

First, a nonlinear autoregressive exogenous model (NARX) provided by MATLAB Neural Net Time Series tool box is considered as a data-driven based machine learning model. The architecture of the NARX is shown in Figure 15, including a hidden layer and an output layer. There are ten nodes in the hidden layer with two delays. The mathematical model of the NARX is shown as (22).

$$y(t) = \text{purelin} \left(B_o + W_o \times \tan \text{sig} \left(\begin{array}{c} B_i + W_i \times X_d(t) \\ + W_l \times Y_d(t) \end{array} \right) \right) \quad (22)$$

where $W_o \in \mathbb{R}^{1 \times 10}$, $W_i \in \mathbb{R}^{10 \times 6}$ and $W_l \in \mathbb{R}^{10 \times 2}$ represents the parameter weight matrices. $B_i \in \mathbb{R}^{10 \times 1}$ and $B_o \in \mathbb{R}^{1 \times 1}$

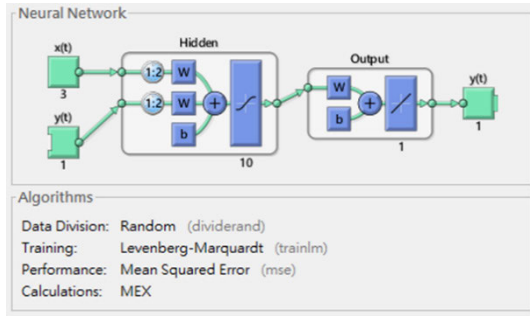


FIGURE 15. Neural network training architecture.

denote the bias of the model. The rest of the variables are defined as follows:

$$\begin{cases} y(t) = \hat{T}_{235}(t), \\ Y_d(t) = \begin{bmatrix} \hat{T}_{235}(t-1) \\ \hat{T}_{235}(t-v2) \end{bmatrix} \end{cases}, \quad X_d = \begin{bmatrix} T_{FANDC}(t-1) \\ N_1(t-1) \\ LPCPR(t-1) \\ T_{FANDC}(t-2) \\ N_1(t-2) \\ LPCPR(t-2) \end{bmatrix} \quad (23)$$

According to the number of input signals and the structure of NARX, there are over 100 parameters have to be identified. Figure 16(a)-(d) show the training results. It can be seen that even if the training data set for those NARXs are the same, the result of each model are different.

To verify the prediction accuracy of the NARXs, a testing dataset, which was not previously included into the training procedure, is used to evaluate the prediction performance of each NARX. The training results and the associated testing results are shown in Figure 16 and Figure 17, respectively. From Figure 16, although most of the training result can reach over 99% of %VAF, the corresponding predictions could be quite different as illustrated in Figure 17.

Apparently, even though the structure of the training model is the same, the training results, including system parameters, and the predictions, are different between models. It reveals that in the use of the data-driven based NN in our case, certain prediction uncertainties exist. Moreover, excessive unknown decision parameters could also increase the risk of overfitting or induced unstable predictions as shown in Figure 17(c).

In the following, the same training and testing procedures are also applied to the proposed physical equation based LPC model to compare the difference between the physical model based modeling and the pure data-driven based NN modeling. The training results and the testing results are illustrated in Figure 18 and Figure 19, respectively.

Recall that the structure of the 3rd-order physical equation based LPC model has evolved from the isentropic compression equation (2). The physical based modeling not only decreases the complexity of the model structure and avoids the uncertainty of parameters but it also prevents the issue of overfitting caused by the NN. Based on the proposed

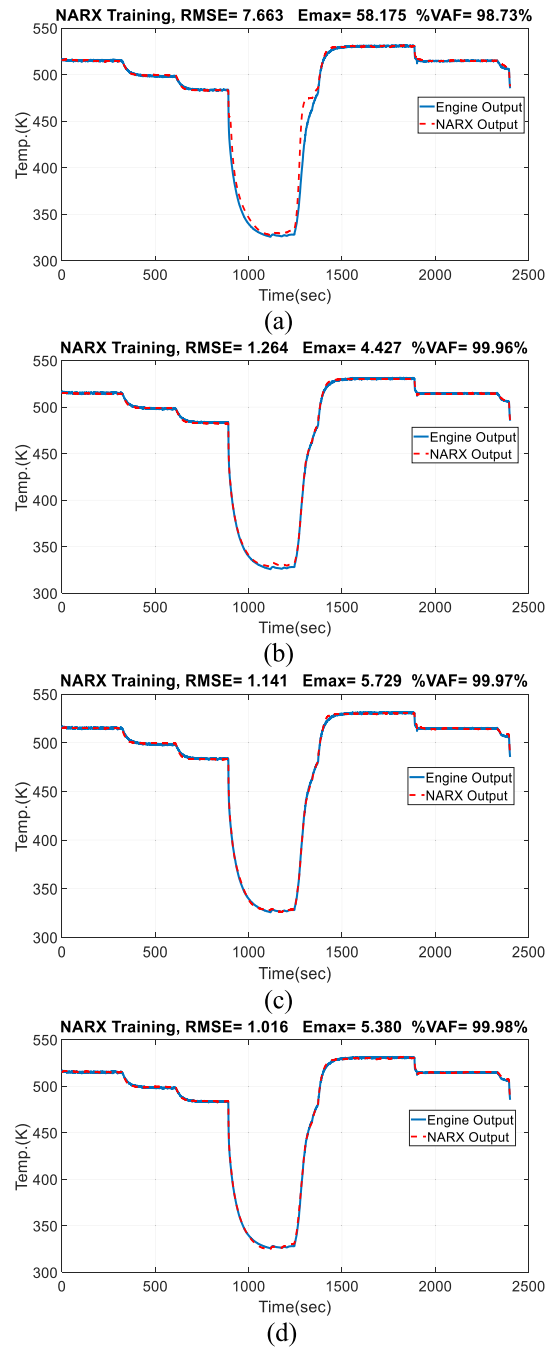


FIGURE 16. Models which trained by data-driven based machine learning.

LPC model, it can be seen that it can achieve high %VAF for both the training/testing results. On the contrary, as shown in Figure 16(c) and Figure 17(c), the training result of NARX model (c), achieves the best fitting and is even greater than the proposed method. Nevertheless, the test result is the worst in all of the NARX's and has an obvious divergence between all the other testing results.

Different from the NN approach, for the same training data set, the resulting estimated model parameters by using the proposed method will remain the same. There is no issue of

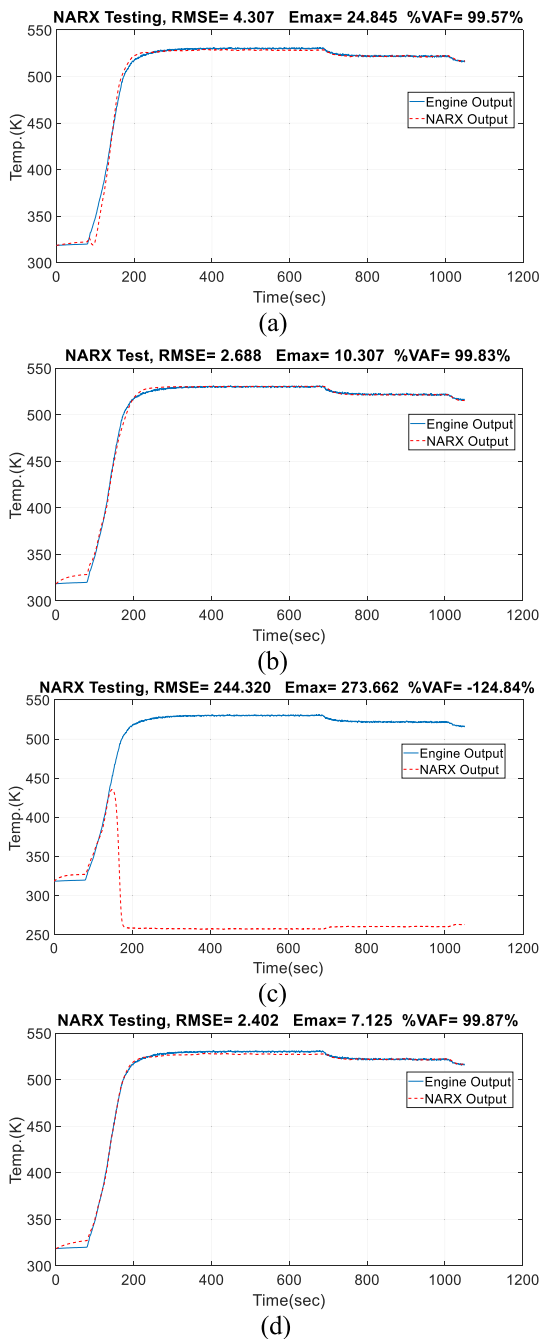


FIGURE 17. Testing result of each NARXs.

parameter uncertainty nor as the result of testing. Moreover, the matching capabilities between the training and testing results are also consistent. Last but not the least, the number of the system parameters from NARX is over 100. Comparing it to NARX, the number of the parameters by using the proposed model is only one-tenth of its quantity. From the perspective of practical implementation and engineering maintenance, it will be a better solution to use less parameters for engine monitoring and status management.

Following experiences consider another training and testing data sets. The training and testing results by using NARXs

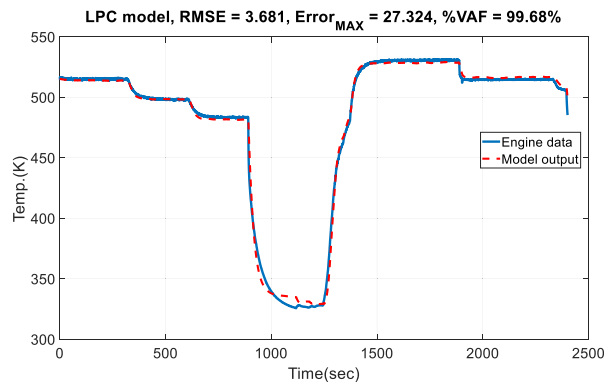


FIGURE 18. Training result of 3rd-order combined LPC model.

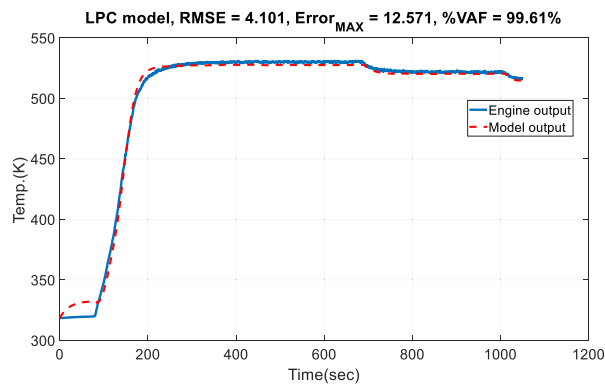


FIGURE 19. Testing result of 3rd-order combined LPC model.

are illustrated in Figure 20 and Figure 21, respectively. It once again demonstrates that there does exist a certain degree of prediction uncertainty when applying the data-driven based NN method.

As illustrated in Figure 20 and Figure 21, part of the data-driven based machine learning results are unstable. Figure 20(b) shows that the inadequate training result is going to cause unreliable predictions as shown in Figure 21(b). However, although the training result is acceptable, as shown in Figure 20(c), the corresponding prediction behaves high RMSE and high maximum prediction error, as shown in Figure 21(c). Comparing it with the proposed LPC model, the physical model based method has a superior stability on both training and testing results.

In conclusion, although the NN is a good method for model training without the use of physical model, it requires huge amount of testing data. Nevertheless, most of the time, the collection of engine test data procedure complex and is costly. The lack of sufficient training data could lead to high uncertainty when using the NN machine learning models. The limited training database will make the pre-trained model hard to recover all the possible operations and thereby lead to unstable prediction results. The huge quantity of parameters in the NN model leads to the unstable performance of the model, increases the risk of overfitting, and makes the training and maintenance cost much higher than the proposed model.

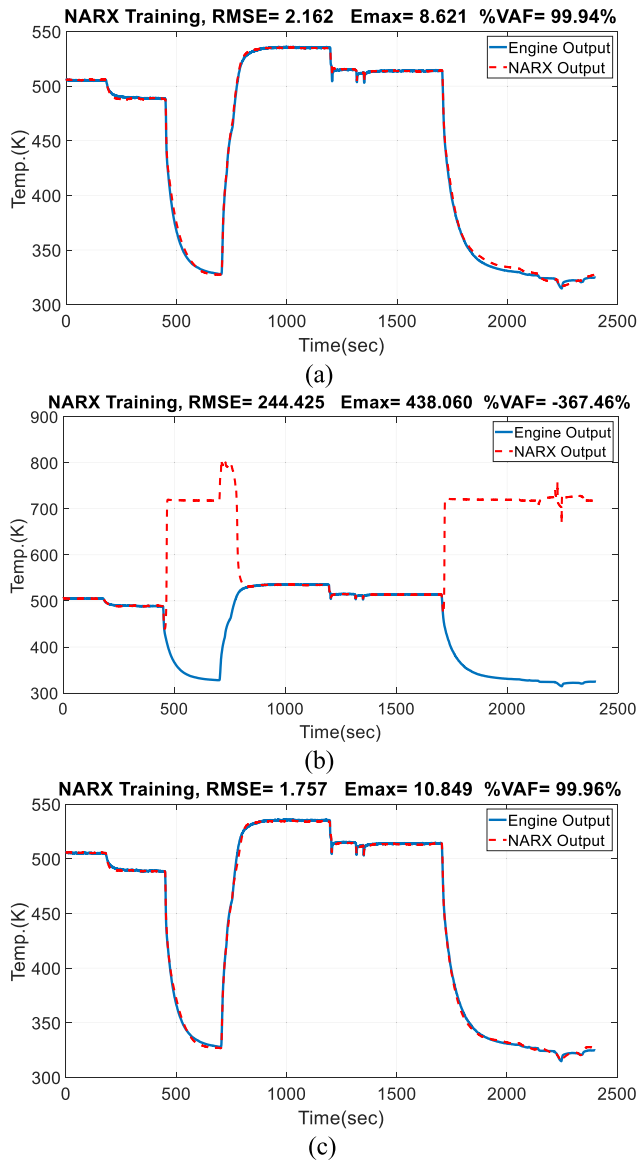


FIGURE 20. Training result of NARXs.

V. OPERATION BOUNDARY GENERATION

The models presented in the previous sections are going to be taken as healthy TFE-731 and are used for behavior prediction as the blue line depicted in Figure 3. Next is to define the upper bound and lower bound of a healthy engine.

There are two popular methods to generate the boundary, including the addition method and the multiplication method. First, the addition method is given in (24), where the boundary is created by adding and subtracting three times of the standard deviation of the system response. Second, the multiplication method is expressed as (25), where the boundary is determined by the output of a healthy model multiplied by a margin parameter. Applying the addition method needs the estimation of σ , which requires huge amount of engine data at different operation points and is not feasible for the current limited database. On the contrary, applying the multiplication

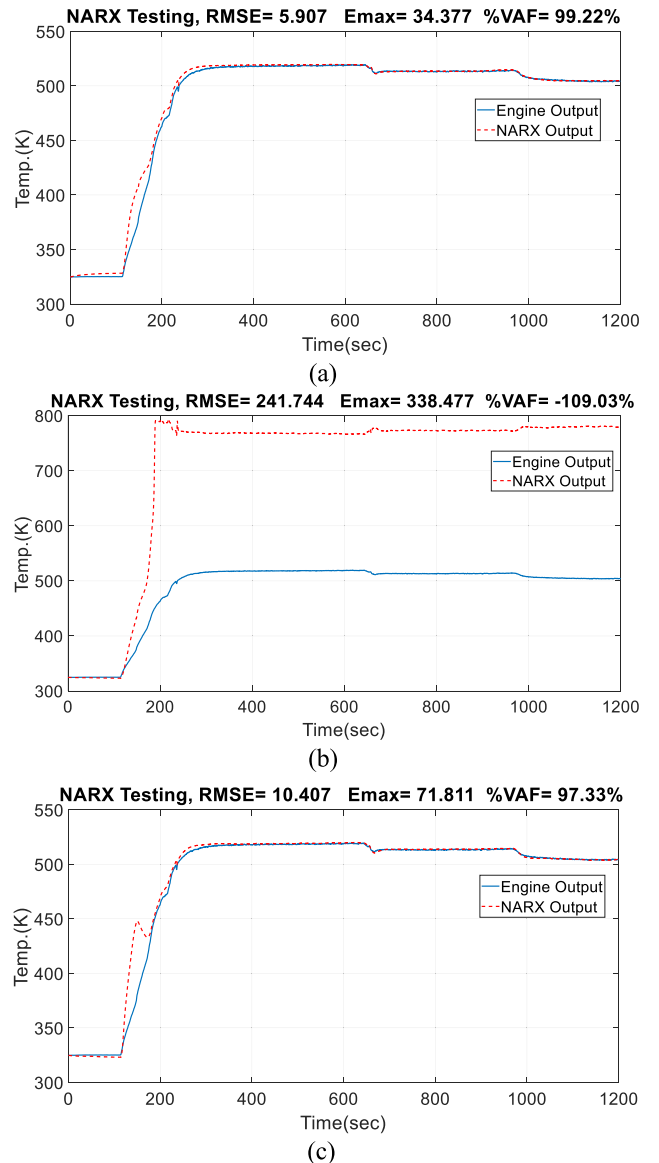


FIGURE 21. Testing result of NARXs.

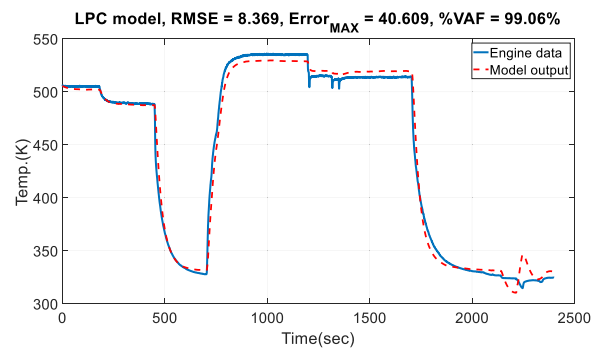


FIGURE 22. Training result of 3rd-order combined LPC model.

method only requires a simple margin parameter. The margin parameter describes the deviation percentage from the reference output and its value can be assigned according to the

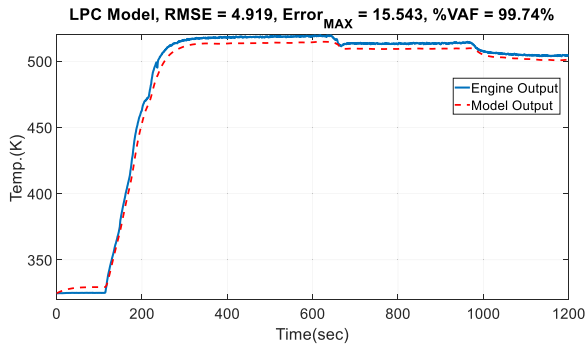


FIGURE 23. Testing result of 3rd-order combined LPC model.

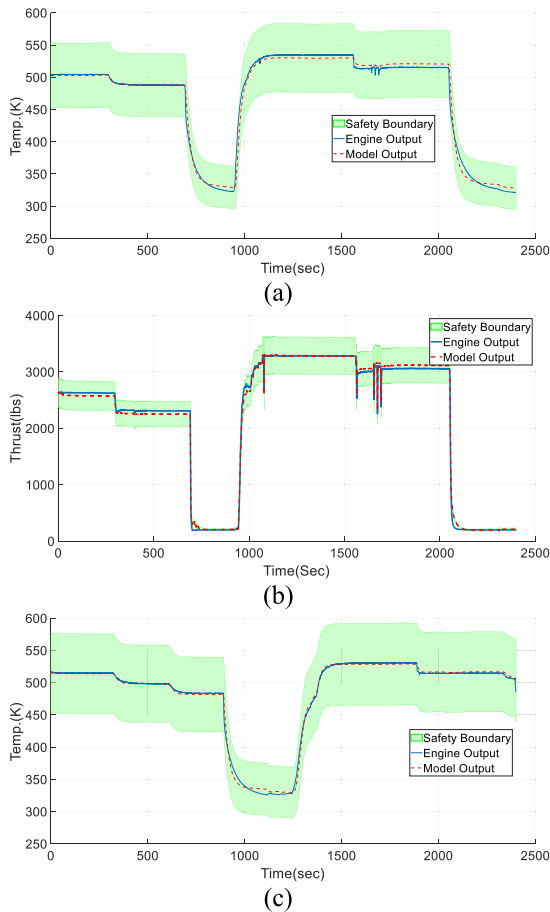


FIGURE 24. LPC model response and safety boundary: (a) ID: 541111 (b) ID: 53130; (c) ID: 86124.

practical maintenance specification.

$$B_A = \text{Modeloutput} \pm 3 \times \sigma \quad (24)$$

$$B_M = \text{Modeloutput} \times (1 \pm \text{MarginParameter}) \quad (25)$$

VI. ON-LINE MONITORING APPLICATION

In the practical operation of a test cell, the proposed real-time condition monitoring system predicts the response of a healthy engine. The monitoring system provides safety boundaries of LPC outlet temperature, HPC outlet

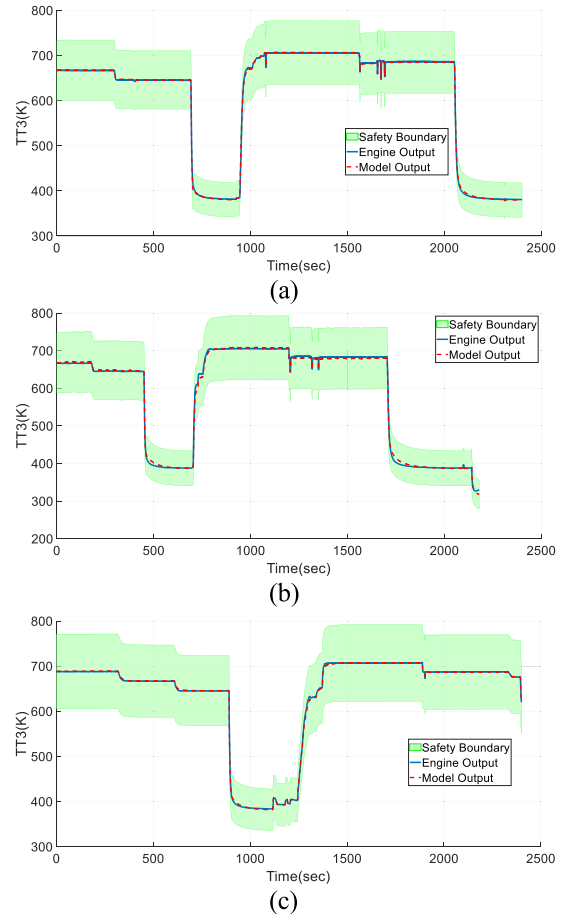


FIGURE 25. HPC model response and safety boundary: (a) ID: 54111; (b) ID: 53130; (c) ID: 86124.

temperature as well as engine thrust. The safety boundaries are created by (25) in real-time, where the margin parameter was set to be 0.12 in this paper. The experiments results are illustrated from Figure 24 to Figure 26. Different from the fixed-threshold mechanism, it shows that once the operator changes the operation status of the TFE-731, the prediction responses and safety boundaries are generated automatically. The proposed model prediction-and-following mechanism facilitates the operator to recognize whether the tested engine is under normal or reasonable status. Width of the safety boundary is varying with the model output, which is the reason that the boundary in overall model cannot be clearly shown during idle thrust.

Moreover, the size of the boundaries can be defined according to the maintenance criterion. The safety boundary can be defined separately as a safe boundary, caution boundary, and a warning boundary for further application and condition monitoring purposes, as shown in Figure 27.

The simplest application is that the engine fault is triggered when the engine responses exceed the red zone. Different from the traditional fixed-threshold monitoring approach, the proposed real-time monitoring system can evaluate the health status for a wide range of operation conditions and

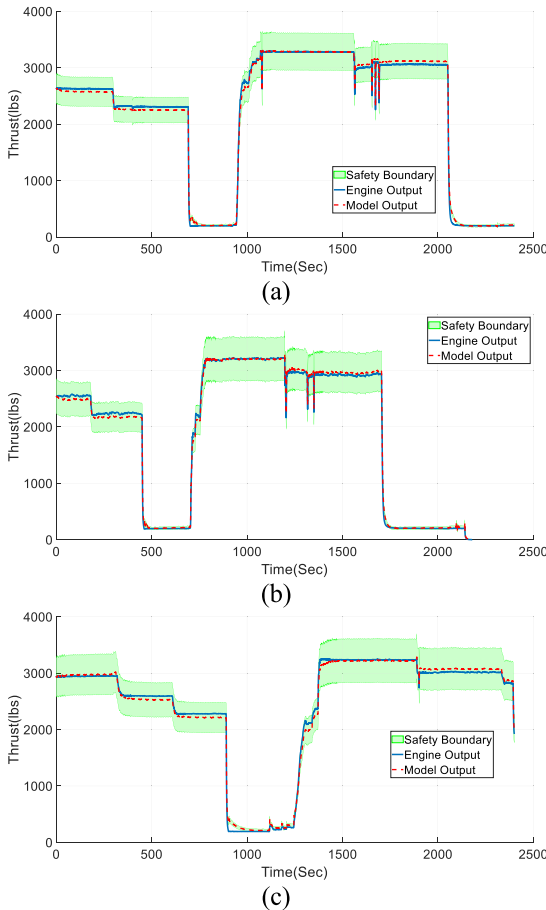


FIGURE 26. Overall model response and safety boundary: (a) ID: 54111; (b) ID: 53130; (c) ID: 86124.

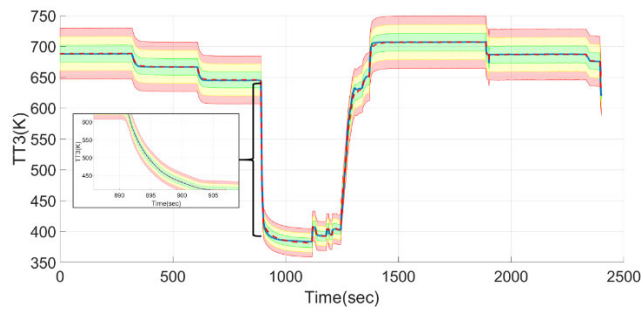


FIGURE 27. Schematic diagram of condition monitoring boundaries.

recognize the occurrence of the failure within a short period of time.

Figure 28 illustrates the final TFE-731 monitoring system architecture for on-line monitoring applications. The local operators can manipulate the engine under different examination demands. Then, the associated output data is collected and fed into the monitoring system in real-time. Once the response of the engine exceeds the safety boundaries, the monitoring system will inform the operator with a warning message or by triggering the relevant lights. It provides clear indicators for maintenance operators to distinguish which

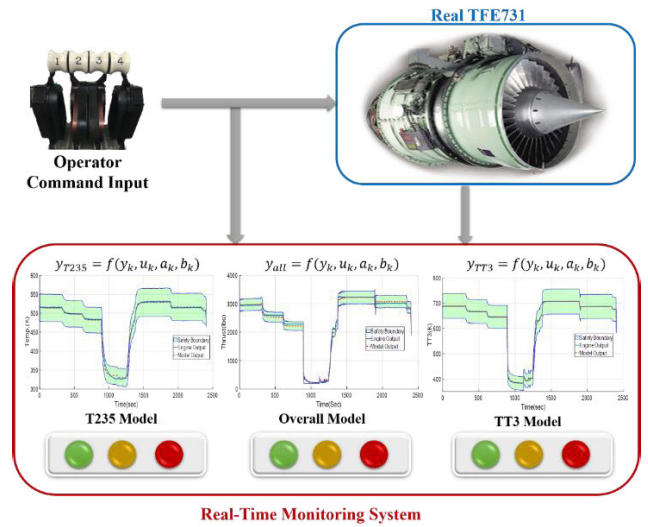


FIGURE 28. Proposed turbofan engine real-time condition monitoring scheme.

engine section is supposed to be scheduled for advanced inspection.

To achieve the real-time monitoring demand, this research focuses on the real-time fault detection of the engine for preventing further damage on the engine. Moreover, it can also reduce the time and the cost of logistics support. Based on the proposed design architecture, it can be used to monitor the real-time performance of unmanned aerial vehicles and other next-generation military systems to enhance operation safety as well as to achieve high maneuverability.

VII. CONCLUSION

To carry out the TFE-731 turbofan engine fault diagnosis, three main engine models are derived and their associated prediction capabilities are presented in this paper. In order to obtain good training and prediction results, an evaluation procedure of the data validation is developed by considering the correlation analysis. Regarding the model derivation, physical models based on the isentropic compression theorem are proposed. In order to enhance model following precision, the regression method as well as fan dynamics are also taken into consideration. The main advantage of the proposed method is that since part of the physical behavior is integrated into the modeling, it reduces the searching of system fitting dimensions and avoids the overfitting problem. In other words, system behaviors can be predicted precisely by using just a few key parameters, which gives great contribution to local maintenance unit. Moreover, parameters identifications are solved by applying the nonlinear optimization process. Comparing between the proposed method and the data-drive based NN method, experiments verify that the developed method can achieve a stable and superior prediction accuracy by using very few parameters. The reduction of both the model complexity and parameters can avoid the risk of overfitting, decrease the real-time calculation load and attenuate maintenance efforts significantly. Finally, all of the turbofan

engine models presented in this research are verified by the real TFE-731 data collected from a test cell. Experiments show that the use of the proposed models for LPC, HPC and overall fan dynamics monitoring are able to achieve stable and precise predictions.

APPENDIX

A PARAMETER SEARCHING ALGORITHM

This section is to present the detail of the LM algorithm for the HPC model parameter estimation. Based on the HPC model (20), definitions of the model outputs and the nonlinear equation can be expressed as below

$$y_n = T_{T3n} \quad (26)$$

$$f_n(\theta^{HPC}) = k_1 \cdot T_{T2n} \cdot LPCPR_n^{k_2} \cdot HPCPR_n^{k_3} + k_4 \cdot N_2 + k_5 \cdot LPCPR_n + k_6 \cdot T_{T2n} + k_7 \cdot HPCPR_n + k_8 \cdot T_{235n} + k_9 \quad (27)$$

The decision variables and the cost function for the optimization process are shown in (28) and (29), respectively.

$$\theta^{HPC} = [k_1, k_2, k_3, k_4, k_5, k_6, k_7, k_8, k_9]^T \quad (28)$$

$$L(\theta^{HPC}) = \sum_{n=1}^N (y_n - f_n(\theta^{HPC}))^2 = \|\mathbf{y} - \mathbf{f}(\theta^{HPC})\|^2 \quad (29)$$

where $\mathbf{y} = [y_1, y_2, \dots, y_N]$ and y_n represent the real HPC outlet temperature. The nonlinear function is defined by $\mathbf{f}(\theta^{HPC}) = [f_1(\theta^{HPC}), f_2(\theta^{HPC}), \dots, f_n(\theta^{HPC})]$, where f_n is the equation of the prediction model.

Let \mathbf{j}_n be the Jacobian matrix of f_n defined as follows

$$(\mathbf{j}_n)_{1 \times 9} = \frac{\partial f_n}{\partial \theta^{HPC}} = \left[\frac{\partial f_n}{\partial k_1}, \frac{\partial f_n}{\partial k_2}, \dots, \frac{\partial f_n}{\partial k_9} \right], \quad n = 1, 2, \dots, N \quad (30)$$

where the definition of each term used in the Jacobian matrix is given as below

$$\begin{aligned} \frac{\partial f_n}{\partial k_1} &= T_{T2n} \cdot LPCPR_n^{k_2} \cdot HPCPR_n^{k_3} \\ \frac{\partial f_n}{\partial k_2} &= k_1 \cdot T_{T2n} \cdot LPCPR_n^{k_2} \cdot HPCPR_n^{k_3} \cdot \log(LPCPR_n) \\ \frac{\partial f_n}{\partial k_3} &= k_1 \cdot T_{T2n} \cdot LPCPR_n^{k_2} \cdot HPCPR_n^{k_3} \cdot \log(HPCPR_n) \\ \frac{\partial f_n}{\partial k_4} &= N_2, \quad \frac{\partial f_n}{\partial k_5} = LPCPR_n, \\ \frac{\partial f_n}{\partial k_6} &= T_{T2n}, \quad \frac{\partial f_n}{\partial k_7} = HPCPR_n, \\ \frac{\partial f_n}{\partial k_8} &= T_{235n}, \quad \frac{\partial f_n}{\partial k_9} = 1 \end{aligned} \quad (31)$$

The data applied in the Jacobian matrix for the iteration could be represented by

$$\mathbf{J}_{N \times 9} = [j_1, j_2, \dots, j_N]^T \quad (32)$$

Note that the selection of the initial values for the LM iteration is based on the isentropic compression model (18). The detail settings are shown in TABLE 5.

From (28)-(32), the system parameter update law is

$$\delta \theta = \left[\mathbf{J}^T \mathbf{J} + \lambda \text{diag}(\mathbf{J}^T \mathbf{J}) \right]^{-1} \mathbf{J}^T (\mathbf{y} - \mathbf{f}) \quad (33)$$

$$\theta_t^{HPC} = \theta_{t-1}^{HPC} + \delta \theta_{t-1}^{HPC} \quad (34)$$

where λ is a damping coefficient used to adjust the convergence rate and to reduce the sensitivity during the iterations.

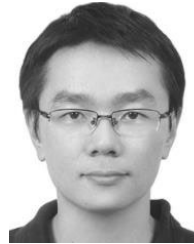
REFERENCES

- [1] M. Kang, S. Ogaji, P. Pilidis, and C. Kong, "An approach to maintenance cost estimation for aircraft engines," *ASME Turbo Expo, Power Land, Sea, Air*, vol. 43116, pp. 71–79, Aug. 2008, doi: [10.1115/GT2008-50564](https://doi.org/10.1115/GT2008-50564).
- [2] H. Saravanamuttoo, H. Cohen, and G. Rogers, *The Turbofan Engine*, 5th ed. London, U.K.: Pearson, 2001.
- [3] T. Hryshchenko. *Integrated Design and Analysis of Turbofan Engines*. [Online]. Available: <http://blog.softinway.com/en/integrated-design-and-analysis-of-turbofan-engines>
- [4] R. Kurz and K. Brun, "Degradation in gas turbine systems," *J. Eng. Gas Turbines Power*, vol. 123, no. 1, pp. 70–77, 2000, doi: [10.1115/1.1340629](https://doi.org/10.1115/1.1340629).
- [5] G. Longbo, Z. Yun, X. Zhipeng, and G. Xiang, "Research on turbofan engine performance seeking control based on the airborne composite model," in *Proc. 4th Int. Conf. Comput. Sci. Netw. Technol. (ICCSNT)*, vol. 1, Dec. 2015, pp. 1524–1528, doi: [10.1109/ICCSNT.2015.7491019](https://doi.org/10.1109/ICCSNT.2015.7491019).
- [6] L. F. Rodriguez and R. M. Botez, "Civil turbofan engines thrust generic model," in *Proc. 38th Annu. Conf. IEEE Ind. Electron. Soc.*, Oct. 2012, pp. 5444–5450, doi: [10.1109/IECON.2012.6389521](https://doi.org/10.1109/IECON.2012.6389521).
- [7] X. Zhang, "Optimization on turbofan engine cycle parameter based on improved differential evolution algorithm," in *Proc. 17th Int. Conf. Control, Automat. Syst. (ICCSAS)*, Oct. 2017, pp. 556–561, doi: [10.23919/ICCSAS.2017.8204296](https://doi.org/10.23919/ICCSAS.2017.8204296).
- [8] M. Yuan, Y. Wu, and L. Lin, "Fault diagnosis and remaining useful life estimation of aero engine using LSTM neural network," in *Proc. IEEE Int. Conf. Aircr. Utility Syst. (AUS)*, Oct. 2016, pp. 135–140, doi: [10.1109/AUS.2016.7748035](https://doi.org/10.1109/AUS.2016.7748035).
- [9] X. Chang, J. Huang, and F. Lu, "Robust in-flight sensor fault diagnostics for aircraft engine based on sliding mode observers," *Sensors*, vol. 17, no. 4, p. 835, Apr. 2017, doi: [10.3390/s17040835](https://doi.org/10.3390/s17040835).
- [10] H.-T. Yau and M. H. Wang, "Chaotic eye-based fault forecasting method for wind power systems," *IET Renew. Power Gener.*, vol. 9, no. 6, pp. 593–599, 2015, doi: [10.1049/iet-rpg.2014.0269](https://doi.org/10.1049/iet-rpg.2014.0269).
- [11] B.-L. Jian, C.-C. Wang, J.-Y. Chang, X.-Y. Su, and H.-T. Yau, "Machine tool chatter identification based on dynamic errors of different self-synchronized chaotic systems of various fractional orders," *IEEE Access*, vol. 7, pp. 67278–67286, 2019, doi: [10.1109/ACCESS.2019.2917094](https://doi.org/10.1109/ACCESS.2019.2917094).
- [12] H.-T. Yau, C.-C. Wang, J.-Y. Chang, and X.-Y. Su, "A study on the application of synchronized chaotic systems of different fractional orders for cutting tool wear diagnosis and identification," *IEEE Access*, vol. 7, pp. 15903–15911, 2019, doi: [10.1109/ACCESS.2019.2894815](https://doi.org/10.1109/ACCESS.2019.2894815).
- [13] W. Gilbert, D. Henrion, J. Bernussou, and D. Boyer, "Polynomial LPV synthesis applied to turbofan engines," *Control Eng. Pract.*, vol. 18, no. 9, pp. 1077–1083, Sep. 2010, doi: [10.1016/j.conengprac.2008.10.019](https://doi.org/10.1016/j.conengprac.2008.10.019).
- [14] L. Reberga, D. Henrion, J. Bernussou, and F. Vary, "LPV modeling of a turbofan engine," *IFAC Proc. Volumes*, vol. 38, no. 1, pp. 526–531, 2005, doi: [10.3182/20050703-6-cz-1902.00488](https://doi.org/10.3182/20050703-6-cz-1902.00488).
- [15] P. Dewallef and K. Mathioudakis, "On-line aircraft engine diagnostic using a soft-constrained Kalman filter," in *Proc. ASME Turbo Expo, Power Land, Sea, Air*, Jan. 2004, pp. 585–594.
- [16] Q. Kun, P. Xiangping, L. Bangyuan, and X. Shousheng, "Kalman filtering with inequality constraints for certain turbofan engine sensors fault diagnosis," in *Proc. 6th World Congr. Intell. Control Automat.*, vol. 2, Jun. 2006, pp. 5428–5432, doi: [10.1109/WCICA.2006.1714109](https://doi.org/10.1109/WCICA.2006.1714109).
- [17] X. Liu and N. Xue, "An improved hybrid Kalman filter design for aircraft engine based on a velocity-based LPV framework," in *Proc. Chin. Control Decis. Conf. (CCDC)*, May 2016, pp. 1873–1878, doi: [10.1109/CCDC.2016.7531288](https://doi.org/10.1109/CCDC.2016.7531288).
- [18] M. A. Boyacioglu and D. Avcı, "An adaptive network-based fuzzy inference system (ANFIS) for the prediction of stock market return: The case of the istanbul stock exchange," *Expert Syst. Appl.*, vol. 37, no. 12, pp. 7908–7912, Dec. 2010, doi: [10.1016/j.eswa.2010.04.045](https://doi.org/10.1016/j.eswa.2010.04.045).

- [19] H.-W. Chiu and C.-H. Lee, "Prediction of machining accuracy and surface quality for CNC machine tools using data driven approach," *Adv. Eng. Softw.*, vol. 114, pp. 246–257, Dec. 2017, doi: [10.1016/j.advengsoft.2017.07.008](https://doi.org/10.1016/j.advengsoft.2017.07.008).
- [20] K. Cai, S. Xie, and K. Zhang, "Neural network model research of some turbofan engine based on recorded flight data," in *Proc. 6th World Congr. Intell. Control Automat.*, vol. 1, Jun. 2006, pp. 1857–1860, doi: [10.1109/WCICA.2006.1712676](https://doi.org/10.1109/WCICA.2006.1712676).
- [21] X. Chang, J. Huang, and F. Lu, "Health parameter estimation with second-order sliding mode observer for a turbofan engine," *Energies*, vol. 10, no. 7, p. 1040, Jul. 2017, doi: [10.3390/en10071040](https://doi.org/10.3390/en10071040).
- [22] D. W. Marquardt, "An algorithm for least-squares estimation of nonlinear parameters," *J. Soc. Ind. Appl. Math.*, vol. 11, no. 2, pp. 431–441, 1963, doi: [10.1137/0111030](https://doi.org/10.1137/0111030).
- [23] J. Lu, F. Lu, and J. Huang, "Performance estimation and fault diagnosis based on Levenberg–Marquardt algorithm for a turbofan engine," *Energies*, vol. 11, no. 1, p. 181, Jan. 2018, doi: [10.3390/en11010181](https://doi.org/10.3390/en11010181).
- [24] Y. Diao and K. M. Passino, "Fault diagnosis for a turbine engine," *Control Eng. Pract.*, vol. 12, no. 9, pp. 1151–1165, Sep. 2004, doi: [10.1016/j.conengprac.2003.11.012](https://doi.org/10.1016/j.conengprac.2003.11.012).
- [25] F. Chang and R. Luus, "A noniterative method for identification using Hammerstein model," *IEEE Trans. Autom. Control*, vol. 16, no. 5, pp. 464–468, Oct. 1971, doi: [10.1109/TAC.1971.1099787](https://doi.org/10.1109/TAC.1971.1099787).
- [26] X.-S. Luo and Y.-D. Song, "Data-driven predictive control of Hammerstein–Wiener systems based on subspace identification," *Inf. Sci.*, vol. 422, pp. 447–461, Jan. 2018, doi: [10.1016/j.ins.2017.09.004](https://doi.org/10.1016/j.ins.2017.09.004).
- [27] J. Frère and F. Hug, "Between-subject variability of muscle synergies during a complex motor skill," *Frontiers Comput. Neurosci.*, vol. 6, p. 99, Dec. 2012.
- [28] R. A. Peterson, "A meta-analysis of variance accounted for and factor loadings in exploratory factor analysis," *Marketing Lett.*, vol. 11, no. 3, pp. 261–275, Aug. 2000, doi: [10.1023/A:1008191211004](https://doi.org/10.1023/A:1008191211004).
- [29] P. Zhao, Y. Dai, and J. Wang, "Performance assessment and optimization of a combined heat and power system based on compressed air energy storage system and humid air turbine cycle," *Energy Convers. Manage.*, vol. 103, pp. 562–572, Oct. 2015, doi: [10.1016/j.enconman.2015.07.004](https://doi.org/10.1016/j.enconman.2015.07.004).
- [30] C.-C. Peng and Y.-I. Lin, "Dynamics modeling and parameter identification of a cooling fan system," in *Proc. IEEE Int. Conf. Adv. Manuf. (ICAM)*, Nov. 2018, pp. 257–260, doi: [10.1109/AMCON.2018.8614957](https://doi.org/10.1109/AMCON.2018.8614957).



SHIH-HUAI CHEN was born in Taipei, Taiwan, in 1994. He received the B.S. degree in system engineering and naval architecture from National Taiwan Ocean University, Keelung, Taiwan, in 2016. He is currently pursuing the M.S. degree with the Institution of Civil Aviation, National Cheng Kung University, Tainan, Taiwan. He was an Exchange Student with École Nationale de l'Aviation Civile, in 2019. His research interests include system modeling, parameter identification, and civil aviation.



CHAO-CHUNG PENG was born in Kaohsiung, Taiwan, in 1980. He received the B.S. degree from the Department of Aeronautics and Astronautics (DAA), National Cheng Kung University (NCKU), Tainan, Taiwan, in 2003, and the Ph.D. degree, in 2009.

From 2008 to 2009, he was a Research Assistant with the Department of Engineering, Leicester University, U.K. From 2010 to 2012, he was a Postdoctoral Fellow at the Department of Mechanical Engineering, NCKU. In 2012, he moved to ADLINK Technology and has served as a Senior Engineer with the Embedded System Development Section, Measurement and Automation Department. From 2014 to 2016, he joined the Automation and Instrumentation System Development Section, Iron and Steel Research and Development Department, China Steel Corporation (CSC). Since 2016, he has been an Assistant Professor with the Department of Aeronautics and Astronautics, NCKU. His research interests include high-performance motion control and applications, unmanned vehicle design and flight control system development, autonomous robotics and intelligence SLAM technology, and system modeling and diagnosis. In 2009, he was awarded a membership in the Phi Tau Phi Scholastic Honor Society.

• • •